DL/CSE/TM65

technical memorandum Daresbury Laboratory

DL/CSE/TM65

SOME ASPECTS OF THE DESIGN OF AMPLIFIERS FOR MULTIWIRE PROPORTIONAL CHAMBERS OPERATING AT HIGH RATES

by

B. V. CAKE
Daresbury Laboratory

JUNE 1977

Science Research Council

Daresbury Laboratory

Daresbury, Warrington WA4 4AD

1. INTRODUCTION

This paper presents an analysis of the factors affecting the signal to noise ratio and pulse response of a multiwire proportional chamber and signal amplifier system. The analysis was performed to establish optimum circuit conditions when using an argon-carbon dioxide gas mixture in beam chambers operating at high incident particle rates per wire. It is well known that the gas gain available with Ar/CO_2 is much lower than that available with 'magic' gas. This leads to small signals from the chamber and a consequent necessity to reduce the amplifier/discriminator threshold by increasing the amplifier gain and reducing the equivalent input noise level. The situation is aggravated by the need to minimise the electronic dead-time and timing jitter.

2. CHAMBER EQUIVALENT CIRCUIT AND OUTPUT PULSE SHAPE

The pulse generated by a chamber is due to the movement, away from the anode wire, of a bunch of positive ions formed very close to the wire during avalanche multiplication. This movement of charge induces a current in the wire. The chamber construction can modify the shape of the output current pulse, but this is noticeable only with very fast (> 150 MHz bandwidth) amplifier systems. For the purposes of this paper it may be assumed that if the signal amplifier rise time is greater than twice the signal propagation time from one end of the wire to the other, then the chamber may be regarded as a capacitive source.

Figure 1 shows the chamber equivalent circuit (one wire only) as a capacitor in parallel with a current generator. The theoretical shape of the current pulse may be derived from ref. 1. The charge build-up on the wire is given by:

$$\frac{Q(t)}{Q_0} = K \log e \left[\frac{t + t_0}{t_0} \right] \qquad (1)$$

where

$Q(t)$ = collected charge at time t.

Q_0 = total charge generated

t_0 = a constant for a given gas (≈ 1.8 ns for A/CO_2)

K = a constant for a fixed value of high voltage.

Differentiating eqn.(1) gives the current:

$$i(t) = \frac{KQ_0}{t_0(1 + t/t_0)} \qquad (2)$$

hence

$$\frac{i(t)}{i(o)} = \frac{1}{1 + t/t_0} \qquad (3)$$

A plot of this is shown in fig. 2. This expression is only approximate, and does not include an expression for the finite rise time of the pulse. However, tests using a signal bandwidth of the order of 5 GHz have shown that the current pulse rise time is of the order of 1-2 ns, so for systems with rise-times greater than this eqn.(3) is adequate.

Figure 3 shows a photograph of current pulses obtained from a small beam chamber with the following construction:

Active area	100 mm x 100 mm
Anode wire diameter	10 μm
Anode wire spacing	1 mm
EHT plane - anode plane spacing	5 mm

The photograph was obtained with a 50/50 Ar/CO_2 gas mixture and an ^{55}Fe x-ray source. Similar pulses have been observed with minimum ionising particles.

The shape of this pulse has been plotted in fig. 2, such that the peak of the measured pulse is centred on the zero time axis. The measured and theoretical pulse shapes are very similar.

Equation 3 is not easy to handle in the response analysis, so an approximation consiting of the sum of two exponential functions will be used:

$$i(t) = i(o) \left[Pe^{-t/T_1} + Qe^{-t/T_2} \right] \qquad (4)$$

A good approximation to the observed pulse is obtained with $P = 0.7$, $Q = 0.3$, $T_1 = 3$ ns, $T_2 = 20$ ns. This is plotted in fig. 4, together with the measured pulse.

3. AMPLIFIER PULSE RESPONSE

There are many different designs of chamber amplifier in use. The chamber load resistance may be any value from a few tens of ohms up to many kilohms. In general, for loads up to 100Ω, grounded base transistor input stages are used. From 100Ω upwards, the input stage normally consists of a grounded emitter transistor with the load resistor connected across the amplifier input. Differential input stages, such as those using MECL gates, are included in the latter category.

The amplifier frequency response will have an upper break point corresponding to its integrating time constant, and will usually have a low frequency break point corresponding to its differentiating time

constant. An equivalent circuit of the amplifier and chamber system is shown in fig. 5. This shows a unity gain voltage amplifier with integrating and differentiating time constants, connected to the chamber load resistance. The analysis is identical if a unity gain current amplifier is connected in series with the load. The response of the system in fig. 5 to a chamber current pulse described by eqn. (4) is given by eqn. 13 in Appendix A. Calculations for various system constants have been performed using a computer program, and the resultant pulse shapes, assuming a 1 μA chamber pulse, are shown in figs. 6-15.

Three load resistor (R) values, 50Ω, 330Ω and 1kΩ, have been taken as representative of current practice. Two values of chamber anode wire capacitance, C, 10 pF and 20 pF, have been assumed. Four differentiating time constants and two integrating time constants are used. The time constant at the amplifier input is denoted by T_3, the integrating time constant by T_4, and the differentiating time constant by T_5.

4. DISCUSSION OF RESPONSE CURVES

Figures 5 and 6 shows the amplifier output pulse shapes with $R = 50\Omega$. Figure 5 applies for $T_4 = 2$ ns and fig. 6 for $T_4 = 5$ ns. These correspond to high frequency break points of 80 MHz and 30 MHz respectively. For these conditions, $T_3 (= R\,C)$ is much shorter than the amplifier integrating time constant and therefore has little effect on the response. From figs. 6 and 7:

1. For $T_5 = \infty$ (amplifier d.c. coupled), the timing jitter, which is a function of the pulse rise time, is about 3.5 ns for $T_4 = 2$ ns, and 6 ns for $T_4 = 5$ ns. In both cases the jitter can be reduced by differentiation, at the expense of peak pulse amplitude. Differentiation

produces a pulse which overswings the zero amplitude axis. This has two effects:

(a) It increases the effective input threshold for a time after the pulse, and this can be serious at high rates.

(b) It increases the adjacent wire trigger rate, since the overswing from a positive pulse induced on an adjacent anode wire is indistinguishable from a negative true signal pulse.

These two drawbacks of differentiation lead to the conclusion that it is undesirable and should be avoided. This does not apply to very long time constant a.c. coupling but care is needed to avoid base-line shift at high rates.

2. The finite bandwidth of the amplifier has two effects:

(a) The pulse is attenuated. Figures 6 and 7 show that with T_4 = 2 ns, the peak voltage referred to R_L is 25 μV ($T_5 = \infty$), and with T_4 = 5 ns, the peak voltage is 17 μV. These correspond to 0.5 μA and 0.34 μA in the load, respectively, for 1 μA chamber pulses.

In real terms this means that, if the threshold of the amplifier-discriminator is checked using a step input, and is set to, say, 1 μA, the true threshold is 2 μA, for T_4 = 2 ns and 3 μA for T_4 = 5 ns.

(b) The 'occupation time', or time during which the amplifier output pulse is over discriminator threshold, increases as T_4 is increased. For comparison, assume that the threshold is 10% of the peak pulse height. For $T_5 = \infty$, figs. 6 and 7 show that with T_4 = 2 ns the pulse is over threshold for 37 ns, and with T_4 = 5 ns it is over threshold for 50 ns. The variation in 'occupation time' is shown graphically in fig. 16. Here the 'occupation time' is shown as a function of threshold for a 10 μA peak amplitude chamber pulse. Since the system dead time can never be less than the 'occupation time', the 'occupation time' governs the efficiency of the system at high rates (assuming no space charge limitation in the chamber).

Much of the foregoing applies to load resistances of 330Ω and 1 kΩ. Figures 8-15 show that the 'occupation time' is considerably increased over that for R = 50Ω. This is due to the effect of T_3 (= R C). The time jitter is also increased.

In general, the response curves show that, to preserve the short 'occupation time' and good timing characteristics of the chamber pulse, the integrating time constants T_3 and T_4 must be kept small. In practical terms this means using a low value of load resistance in order to reduce T_3, and using wide band amplifiers to reduce T_4.

It should be noted here that the efficiency of the chamber-amplifier system is not simply governed by the electronic dead-time. At high rates, space charge effects in the chamber reduce the gas gain[2]. The positive ions drifting towards the cathode reduce the field at the anode and this reduces the gas gain. Now, if the amplifier-discriminator threshold is reduced, and the EHT is reduced to reduce the gas gain by the same factor, then at a fixed particle rate the number of positive ions drifting towards the cathode is also reduced by the same factor. This would allow an increase in particle rate before inefficiency due to space charge commences. In simple terms, a reduction of threshold by a factor of two, combined with a change in EHT to reduce the gas gain by a factor of two, should allow operation at twice the particle rate for the same

inefficiency[3]. Therefore the amplifier-discriminator threshold should be reduced to the smallest possible level consistent with noise, interference and economic consideration if operation at high rates is required.

5. NOISE PERFORMANCE OF MWPC AMPLIFIERS

The noise generated by the chamber amplifier sets an absolute lower limit to the achievable threshold. The analysis presented here was performed in order to establish this limit so that amplifier gain and discriminator threshold may be chosen. It also allows optimisation of the amplifier input circuit for best signal-noise ratio.

5.1 Grounded Base Low Input Impedance Stage

The noise analysis of this stage is detailed in section 1 of Appendix B, and shows that the equivalent rms noise current at the input of a grounded base amplifier followed by a single integrating time content is given by:

$$\sqrt{i_0^2} = \left[\frac{k_T (r_b + \frac{r_e}{2}) C^2}{T_3 T_4 (T_3 + T_4)} + \frac{q I_b}{2(T_3 + T_4)} \right]^{\frac{1}{2}} \qquad (5)$$

where

$\sqrt{i_0^2}$ = rms noise current

k = Boltzmann's constant

T = absolute temperature.

r_b = transistor base resistance

r_e = transistor emitter resistance

I_b = transistor d.c. base current

q = charge on an electron.

It is important to note that the noise voltage generated by the emitter resistance is lower, by a factor of $\sqrt{2}$, than that generated by an equivalent 'real' resistance. For this reason, the use of a grounded base input stage can reduce the threshold below that achievable with a discrete load resistor of the same value. Care must be taken in the selection of the input transistor, since its r_b generates full thermal noise, so devices with low r_b must be used. Typical of these are the BFY90 and BFW30, with r_b of order 10Ω and f_T is excess of 1 GHz.

Table 1 shows the calculated and measured equivalent input noise current for a BFY90 grounded base stage, with r_e = 50Ω, C = 10 pF and 20 pF, and T_4 = 2 ns and 5 ns. For the measurements, the stage was followed by a low noise current amplifier.

The measured results are in reasonable agreement with calculation considering that r_b is not accurately known and no contribution from the bulk emitter resistance is assumed. The peak noise current in Table 1 is only approximate, since measurement of the peak current must be related to the noise count rate. However, taking the peak noise as equal to 2.5 x the rms noise is a convenient measure of peak noise amplitude. The peak noise amplitude determines the minimum threshold current, and from Table 1 it can be seen that a threshold of approximately 0.2 μA is attainable. For T_4 = 2 ns, C = 20 pF and $T_5 = \infty$, this corresponds to a true input threshold of approximately 0.4 μA.

5.2 High Impedance Grounded Emitter Stage

The analysis of this stage is included for completeness, since it has already been shown that the pulse response is much poorer than the grounded base stage, when operation at high rates is required.

The noise analysis is given in section 2 of Appendix B. This shows that the equivalent rms noise voltage generated at its input is given approximately by:

$$\sqrt{V_i^2} = \left[\frac{1}{4(T_3 + T_4)} \left(\frac{2kTR^2}{\beta r_e} + 4kTR \right) + \frac{1}{4T_4} \left(\frac{2kTr_b^2}{\beta r_e} + 2kTr_e + 4kTr_b \right) \right]^{\frac{1}{2}} \quad (6)$$

This assumes that the common emitter current gain, β, does not vary with frequency, and that the stage input impedance is high compared with the input load resistor, R.

Table 2 shows the results of calculation and measurement for this type of input stage using a BFY90 transistor.

Taking the frequency at which the common emitter current gain is unity, f_T, of a BFY90 with ½ mA collector current as 1 GHz, then:

$$Z_{in} \doteqdot \frac{f_T}{f} \times r_e$$

where

Z_{in} = base input inpedance

f = frequency.

For f = 30 MHz, $Z_{in} \doteqdot 1.7$ k , so for an amplifier bandwidth of 30 MHz, eqn.(6) is tolerably accurate. T_4 is fixed at 5 ns, since reducing it below this value gains little in pulse amplitude, but increases the amplifier noise contribution. The agreement between measured and calculated noise amplitude is reasonable considering the approximation made in deriving eqn.(6). Table 2 shows that a noise-limited threshold of

approximately 60 μV should be possible. The corresponding true chamber thresholds are also shown in Table 3. This shows that, for R = 1 kΩ, the minimum true threshold is approximately the same as for the grounded base input stage. With R = 330Ω, the achievable threshold increases significantly.

6. POLE-ZERO COMPENSATION TECHNIQUES

A short mention will be made here of the application of pole-zero compensation to chamber pulses, since this allows a significant reduction of the 'occupation time' without introducing serious pulse undershoot. A detailed review of the technique is given elsewhere[4].

A full analysis of compensation using CR networks is given in Appendix C, and the response to a chamber pulse is shown in fig. 17. This shows a considerable reduction in 'occupation time' without serious attenuation or undershoot. It may be possible to use pole-zero compensation to reduce the 'occupation time' in systems with high chamber load resistances, but this has not been explored by the author.

No attempt has been made by the author to recalculate the noise performance of the amplifier with pole-zero shaping. However, if the shaping is included in the amplifier at a point where noise contribution from the compensation components is negligible, then the noise should be reduced, since the network reduces the low frequency amplifier gain. This reduction in noise level would be small since the majority of the noise is distributed at the high frequency part of the spectrum.

CONCLUSIONS

This paper has analyzed signal and noise considerations in fast proportional chamber amplifiers. The analysis allows the calculation of the performance for two common types of input stage, and shows that a low impedance grounded base stage, followed by a fast current amplifier with pole-zero shaping can produce an input threshold sensitivity of considerably less than 1 μA. The dead-time can be less than 20 ns for 10 x overdrive, with a time-jitter of less than 5 ns.

This analysis has been used in the design of an amplifier-disciminator circuit for use with 100 mm x 100 mm beam chambers, at a total beam rate of 10^7/second (electrons). The maximum rate per wire is ≈ 5 x 10^5/second. Preliminary tests of the amplifier in an electron beam are detailed elsewhere[4].

During the development of the amplifier-discriminator system, it was found that the theoretical threshold is achievable in practice for single channel systems. Interference and cross-talk problems become serious when many channels are used, since it is not possible to individually screen each channel, for economic reasons.

ACKNOWLEDGEMENTS

The advice and assistance of a considerable number of colleagues at Daresbury Laboratory and the Physics Department of Manchester University is gratefully acknowledged. Mr D Clarke of Daresbury Laboratory (now with the Rutherford Laboratory) suggested the use of pole-zero compensation and wrote the computer program for the evaluation of pulse shapes.

APPENDIX A

DERIVATION OF PULSE SHAPE AND AMPLITUDE FROM OUTPUT OF CHAMBER AND AMPLIFIER

Consider the amplifier block diagram shown in fig. 5. This shows a complete chamber and amplifier system with all the amplifier transfer functions. From fig. 5:

$$V_0(s) = \frac{i(s)\, R\, sT_5}{(1 + sT_3)(1 + sT_4)(1 + sT_5)} \tag{7}$$

Since it is assumed that the amplifier has unity gain, this is an expression for the equivalent input voltage.

From eqn.(4):

$$\begin{aligned} i(s) &= \mathcal{L}\, i_0 \left[Pe^{-t/T_1} + Qe^{-t/T_2} \right] \\ &= i_0 \left[\frac{PT_1}{1 + sT_1} + \frac{QT_2}{1 + sT_2} \right] \end{aligned} \tag{8}$$

Combining eqns.(7) and (8):

$$V_0(s) = i_0 R \left[\frac{PT_1}{1 + sT_1} + \frac{QT_2}{1 + sT_2} \right] \left[\frac{sT_5}{(1 + sT_3)(1 + sT_4)(1 + sT_5)} \right] \tag{9}$$

Now let

$$\frac{T_4}{T_5} = A, \quad \frac{T_3}{T_1} = B, \quad \frac{T_5}{T_1} = C,$$

$$\frac{T_4}{T_1} = D, \quad \frac{T_4}{T_3} = E, \quad \frac{T_5}{T_3} = F,$$

$$\frac{T_3}{T_2} = G, \quad \frac{T_5}{T_2} = H, \quad \frac{T_4}{T_2} = J.$$

then:

$$V_0(t) = \frac{i_0 RP}{(A-1)(1-B)} \left[e^{-t/T_1} \left[\frac{1}{1-C} - \frac{1}{1-D} \right] \right.$$

$$+ e^{-t/BT_1} \left[\frac{1}{1-E} - \frac{1}{1-F} \right] + e^{-t/DT_1} \left[\frac{1}{1-D} - \frac{1}{1-E} \right]$$

$$\left. + e^{-t/CT_1} \left[\frac{1}{1-F} - \frac{1}{1-C} \right] \right] \qquad (10)$$

$$+ \frac{i_0 RQ}{(A-1)(1-G)} \left[e^{-t/T_2} \left[\frac{1}{1-H} - \frac{1}{1-J} \right] + e^{-t/GT_2} \left[\frac{1}{1-E} - \frac{1}{1-F} \right] \right.$$

$$\left. + e^{-t/JT_2} \left[\frac{1}{1-J} - \frac{1}{1-E} \right] + e^{-t/HT_2} \left[\frac{1}{1-F} - \frac{1}{1-H} \right] \right]$$

for constants A, ..., J $\neq$ 1.

APPENDIX B

ELECTRONIC NOISE CALCULATIONS FOR MWPC AMPLIFIERS

1. GROUNDED BASE LOW INPUT IMPEDANCE AMPLIFIER

Figure 17 shows the basic circuit of the amplifier to be analyzed. Transistor J_1 is connected in grounded base, and if this stage feeds a low input impedance amplifier, the input impedance of J_1 is given by:

$$Z_{in} = r_e + \frac{r_b}{h_{fe}} \doteq \frac{25 \times 10^{-3}}{I_{dc}} + \frac{r_b}{h_{fe}} \qquad (11)$$

where r_e = emitter resistance, r_b = base resistance, h_{fe} = current gain of J_1 at the measurement frequency.

Figure 19 is an equivalent circuit showing all significant noise generators, assuming that the current amplifier bandwidth, defined by T_4, is much less than the f_T of J_1.

All the noise generators are assumed to have constant spectral density, and are expressed as V^2/Hz or A^2/Hz. It will be assumed that the gain of the current amplifier is unity, thus referring the calculated noise to the input. Noise generated by the current amplifier is assumed to be insignificant.

From fig. 19, ignoring initially the contribution from $\overline{i_b^2}$:

$$i_c^2\Big|_\omega = \frac{1}{2\pi} \frac{(\overline{e_b^2} + \overline{e_e^2})}{(r_e + \frac{1}{j\omega C})^2} \delta\omega \, A^2 \qquad (12)$$

This assumes that the β of $J_1 \gg 1$.

Putting $\overline{e^2} = \overline{e_b^2} + \overline{e_e^2}$

$$\left.\overline{i_c^2}\right|_\omega = \frac{\overline{e^2}}{2\pi}\left[\frac{j\omega C}{1 + j\omega T_3}\right]^2 \delta\omega \quad A^2 \tag{13}$$

where $T_3 = r_e C$.

The transfer function, $G(\omega)$, for a simple integrator with time constant T_4 is given by:

$$G(\omega) = \frac{1}{1 + j\omega T_4} \tag{14}$$

Therefore the mean square amplifier output, $\overline{i_0^2}$, is given by:

$$\left.\overline{i_0^2}\right|_\omega = \overline{i_c^2}\, G^2(\omega) = \frac{\overline{e^2}}{2\pi}\left[\frac{\omega^2 C^2}{1 + \omega^2 T_3^2} \cdot \frac{1}{1 + \omega^2 T_4^2}\right] \delta\omega \tag{15}$$

Integrating over the angular frequency range o to ∞

$$\overline{i_0^2} = \frac{\overline{e^2}}{2\pi}\,\frac{C^2}{T_3^2}\int_0^\infty \frac{\omega^2 T_3^2}{(1 + \omega^2 T_3^2)(1 + \omega^2 T_4^2)}\, d\omega = \frac{\overline{e^2}\, C^2}{4T_3\, T_4(T_3 + T_4)} \tag{16}$$

now

$$\overline{e^2} = \overline{e_e^2} + \overline{e_b^2}$$

$$\overline{e_e^2} = 2kTr_e$$

$$\overline{e_b^2} = 4kTr_b$$

where

k = Boltzmann's constant

T = absolute temperature

$$\overline{i_0^2} = \frac{kT(r_b + \frac{r_e}{2})\, C^2}{T_3\, T_4(T_3 + T_4)} \quad A^2 \tag{17}$$

This is the mean square output current due to the noise generated by r_b and r_e. In a similar manner, the mean square current due to the base current may be calculated. The base current in a junction transistor generates full shot noise which is uncorrelated with the emitter resistance and base resistance noise. It appears as an equivalent current noise source connected across the input, as shown in fig. 19.

Now

$$\overline{i_b^2} = 2q\, I_b \quad A^2/Hz \tag{18}$$

where

q = electronic charge

I_b = d.c. base current of J_1

$$\left.i_0^2\right|_\omega = \frac{\overline{i_b^2}}{2\pi}\,\frac{1}{(1 + \omega^2 T_3^2)(1 + \omega^2 T_4^2)}\, \delta\omega \tag{19}$$

and integrating as before:

$$\overline{i_0^2} = \frac{\overline{i_b^2}}{4(T_3 + T_4)} \tag{20}$$

Therefore $\overline{i_0^2}$ due to base current

$$\overline{i_0^2} = \frac{2q\, I_b}{4(T_3 + T_4)} \tag{21}$$

Therefore the total noise output is the sum of eqns. (17) and (21).

$$\sqrt{\overline{i_0^2}} = \left[\frac{kT(r_b + \frac{r_e}{2})C^2}{T_3 T_4 (T_3 + T_4)} + \frac{q I_b}{2(T_3 + T_4)} \right]^{\frac{1}{2}} \qquad (22)$$

2. GROUNDED EMITTER INPUT STAGE

This analysis considers the case of a grounded emitter stage with the chamber load defined by a resistor connected across the amplifier input, as shown in fig. 20. It will be assumed that the input impedance of the amplifier following the input stage is low so that collector-base feedback around the input stage is insignificant. Figure 21 shows the noise equivalent circuit, where $\overline{e_e^2}$, $\overline{e_b^2}$ and $\overline{e_R^2}$ are the mean square noise voltages per Hz generated by r_e, r_b and R respectively, and $\overline{i_b^2}$ is the mean square shot noise current per Hz generated by the d.c. base current I_b. It will be assumed that βr_e, the input impedance of J_1, is large compared with R and r_b. The noise bandwidth is defined by T_4 in the second amplifier. Figure 21 may be redrawn as in fig. 22.

The analysis is performed exactly as for the grounded base stage and yields:

$$\overline{i_0^2} = \frac{\overline{i_b^2}}{r_e^2}\left[\frac{R^2}{4(T_3 + T_4)} + \frac{r_b^2}{4T_4}\right] + \frac{1}{4T_4}\left[\frac{\overline{e_e^2}}{r_e^2} + \frac{\overline{e_b^2}}{r_b^2}\right] + \frac{\overline{e_R^2}}{r_e^2}\,\frac{1}{4(T_3 + T_4)} \qquad (23)$$

where $T_3 = RC$.

Now

$$\overline{e_e^2} = 2kTr_e$$

$$\overline{e_b^2} = 4kTr_b$$

$$\overline{e_R^2} = 4kTR$$

$$\overline{i_b^2} = \frac{2q I_e}{\beta}$$

and since

$$r_e = \frac{kT}{qI_e}$$

then

$$\overline{i_b^2} = \frac{2kT}{\beta r_e}$$

Substituting in eqn. (23)

$$\overline{i_0^2} = \frac{1}{r_e^2}\left[\frac{1}{4(T_3 + T_4)}\left(\frac{2kTR^2}{\beta r_e} + 4kTR\right) + \frac{1}{4T_4}\left(\frac{2kTr_b^2}{\beta r_e} + 2kTr_e + 4kTr_b\right)\right] \qquad (24)$$

The equivalent input noise voltage, $\overline{V_i^2}$, is given by:

$$\overline{V_i^2} = \frac{i_0^2}{g_m^2} = \overline{i_0^2}\, r_e^2$$

Therefore

$$\sqrt{\overline{V_i^2}} = \left[\frac{1}{4(T_3 + T_4)}\left(\frac{2kTR^2}{\beta r_e} + 4kTR\right) + \frac{1}{4T_4}\left(\frac{2kTr_b^2}{\beta r_e} + 2kTr_e + 4kTr_b\right)\right]^{\frac{1}{2}} \qquad (25)$$

APPENDIX C

THE APPLICATION OF POLE-ZERO COMPENSATION TECHNIQUES

MWPC AMPLIFIERS

In this Appendix, the application of a particular type of compensation to fast amplifiers will be analyzed. Figure 23 shows a CR network connected between two stages in the amplifier. The current into the second of the two stages is given by:

$$i_2(s) = \frac{i(s)\ R_1}{R_1 + R_2}\left[\frac{1 + sT_6}{1 + sT_7}\right] \qquad (26)$$

where

$$T_6 = CR_2$$

$$T_7 = \frac{CR_1R_2}{R_1 + R_2}$$

Putting $T_6 = nT_7$, then

$$\frac{R_1}{R_1 + R_2} = \frac{1}{n}$$

From Appendix A

$$i(s) = i(o)\left[\frac{PT_2}{1 + sT_1} + \frac{QT_2}{1 + sT_2}\right]$$

$$i_2(s) = \frac{i(o)}{n}\left[\frac{PT_1}{1 + sT_1} + \frac{QT_2}{1 + sT_2}\right]\left[\frac{1 + sT_6}{1 + sT_7}\right]$$

Finding the inverse transform and referring the current pulse back to an equivalent voltage pulse at the amplifier input:

$$V_0(t) = \frac{i(o)\ R}{n}\left[Pe^{-t/T_1}\left[\frac{1 - \frac{nT_7}{T_1}}{1 - \frac{T_7}{T_1}}\right] + Qe^{-t/T_2}\left[\frac{1 - \frac{nT_7}{T_2}}{1 - \frac{T_7}{T_2}}\right] + e^{-t/T_7}\left[\frac{P(n-1)}{1 - \frac{T_7}{T_1}} + \frac{Q(n-1)}{1 - \frac{T_7}{T_2}}\right]\right] \qquad (27)$$

This assumes that T_3 is negligibly small, i.e. R < 100Ω. Now let $nT_7 = T_2$, thus removing the component in e^{-t/T_2}

$$V_0(t) = \frac{i(o)R}{n}\left[Pe^{-t/T_1}\left[\frac{1 - \frac{nT_7}{T_1}}{1 - \frac{T_7}{T_1}}\right] + e^{-t/T_7}\left[\frac{P(n-1)}{1 - \frac{T_7}{T_1}} + \frac{Q(n-1)}{1 - \frac{1}{n}}\right]\right] \qquad (28)$$

Equation (28) gives the pulse response before integration by the amplifier. In allowing for the effect of T_4, the following expression results.

$$V_0(t) = \frac{i(o)\,R_L}{n}\left[\frac{KPe^{-t/T_1}}{1-\frac{T_4}{T_1}} + \frac{LQe^{-t/T_2}}{1-\frac{T_4}{T_2}} + \frac{(MP+NQ)\,e^{-t/T_7}}{1-\frac{T_4}{T_7}} - e^{-t/T_4}\left[\frac{KP}{1-\frac{T_4}{T_1}} + \frac{LQ}{1-\frac{T_4}{T_2}} + \frac{(MP+NQ)}{1-\frac{T_4}{T_7}}\right]\right] \quad (29)$$

where

$$K = \frac{1-\frac{nT_7}{T_1}}{1-\frac{T_7}{T_1}}, \qquad L = \frac{1-\frac{nT_7}{T_2}}{1-\frac{T_7}{T_2}}$$

$$M = \frac{n-1}{1-\frac{T_7}{T_1}}, \qquad N = \frac{n-1}{1-\frac{T_7}{T_2}}$$

A plot of the response given by eqn.(29), with n = 4 (T_7 = 5 ns), T_4 = 2 ns, R = 50Ω is shown in fig. 17. This shows the response to a 1 μA chamber pulse. Also shown are curves for T_7 = 2.5 ns and T_7 = 7.5 ns, in a first attempt at establishing the sensitivity of the compensation to changes in chamber pulse shape and compensation network changes. The maximum pulse attenuation, with T_7 = 2.5 ns, is 32% over the uncompensated response. The maximum percentage underswing, with T_7 = 7.5 ns, is 4.7%, giving a positive pulse rejection of about 20 : 1, a reasonably acceptable figure. Figure 17 shows clearly that very considerable reduction of 'occupation time' may be achieved with simple passive compensation, with very little effect on amplitude, and with an acceptable pulse underswing.

REFERENCES

1. G. Charpak, D. Rahn and H. Steiner, Nucl. Instr. and Meth. 80 (1970) 13.

2. B Sadoulet and B Makowski, CERN Report. CERN/D.Ph.II/PHYS-7B-3 (1973).

3. I P Duerdoth, R J Ellison, R E H Jones, D Mercer, B V Cake and D Clarke, Nucl Instr. and Meth. 129 (1975) 461.

4. G Amsel, R Bosshard and C Zajde, Nucl. Instr. and Meth. 71 (1969) 1.

Table 1

Calculated and Measured Equivalent Input Noise Current for BFY90

Grounded Base Input Stage. $\beta = 60$, $r_b = 10\Omega$, $r_e = 50\Omega$.

T_4	C	$\sqrt{i_0^2}$ Calculated μA	$\sqrt{i_0^2}$ Measured μA	i_0 peak Measured μA
5 ns	10 pF	0.033	0.05	0.13
5 ns	20 pF	0.044	0.057	0.14
2 ns	10 pF	0.076	0.07	0.18
2 ns	20 pF	0.097	0.08	0.2

Table 2

Calculated and Measured Equivalent Input Noise Voltage for Grounded Emitter Input Stage BFY90 ($r_e = 50\Omega$, $r_b = 10\Omega$, $\beta = 60$, $T_4 = 5$ ns)

R	C	$\sqrt{V_i^2}$ Calculated μV	$\sqrt{V_i^2}$ Measured μV	V_i peak Measured μV
1 kΩ	10 pF	18	26	65
1 kΩ	20 pF	14	22	55
330Ω	10 pF	14	20	50
330Ω	20 pF	12	18	45

Table 3

True Chamber Pulse Threshold Current for Grounded Emitter Input Stage

($T_4 = 5$ ns, $r_e = 50\Omega$, $r_b = 10\Omega$, $\beta = 60$) BFY90.

R	C	True Threshold μA
1 kΩ	10 pF	0.3
1 kΩ	20 pF	0.4
330Ω	10 pF	0.6
330Ω	20 pF	0.8

FIGURE CAPTIONS

Fig. 1 Chamber equivalent circuit.

Fig. 2 Comparison of measured (⊗) and theoretical (x) chamber pulses.

Fig. 3 Measured chamber pulse. Ar/CO_2 mixture (50 : 50). ^{55}Fe x-ray source. 50 mV/cm, 20 ns/cm.

Fig. 4 Comparison of measured (Δ) and approximated (x) chamber pulses.

Fig. 5 Chamber and amplifier equivalent circuit.

Fig. 6 Calculated output pulse for 1 μA chamber pulse. R = 50Ω, C = 10 pF, T_4 = 2 ns.

Fig. 7 Calculated output pulse for 1 μA chamber pulse. R = 50Ω, C = 10 pF, T_4 = 5 ns.

Fig. 8 Calculated output pulse for 1 μA chamber pulse. R = 1 kΩ, C = 10 pF, T_4 = 2 ns.

Fig. 9 Calculated output pulse for 1 μA chamber pulse. R = 1 kΩ, C = 10 pF, T_4 = 5 ns.

Fig. 10 Calculated output pulse for 1 μA chamber pulse. R = 1 kΩ, C = 20 pF, T_4 = 2 ns.

Fig. 11 Calculated output pulse for 1 μA chamber pulse. R = 1 kΩ, C = 20 pF, T_4 = 5 ns.

Fig. 12 Calculated output pulse for 1 μA chamber pulse. R = 330Ω, C = 10 pF, T_4 = 2 ns.

Fig. 13 Calculated output pulse for 1 μA chamber pulse. R = 330Ω, C = 10 pF, T_4 = 5 ns.

Fig. 14 Calculated output pulse for 1 μA chamber pulse. R = 330Ω, C = 20 pF, T_4 = 2 ns.

Fig. 15 Calculated output pulse for 1 μA chamber pulse. R = 330Ω, C = 20 pF, T_4 = 5 ns.

Fig. 16 Variation of 'occupation time' with threshold. 10 μA chamber pulse, R = 50Ω, C = 10 pF, $T_5 = \infty$.

Fig. 17 Effect of pole-zero compensation on chamber pulse. 1 μA chamber pulse, T_4 = 2 ns, R = 50Ω, C = 10 pF, T_6 = 20 ns.

Fig. 18 Grounded base input stage. W is a low input-impedance noiseless current amplifier with integrating time constant defined by T_4.

Fig. 19 Grounded base input stage showing noise sources.

Fig. 20 Grounded emitter input stage. W is as in fig. 18.

Fig. 21 Grounded emitter stage showing noise sources.

Fig. 22 Equivalent circuit for fig. 21.

Fig. 23 Pole-zero network connected between two current amplifier stages.

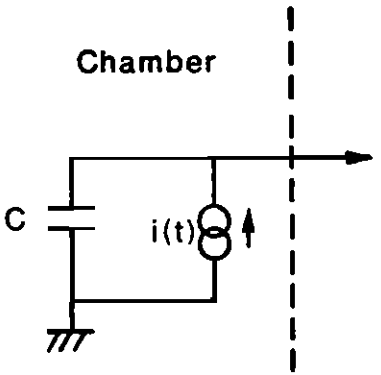
Chamber
C
i(t)

Fig. 1

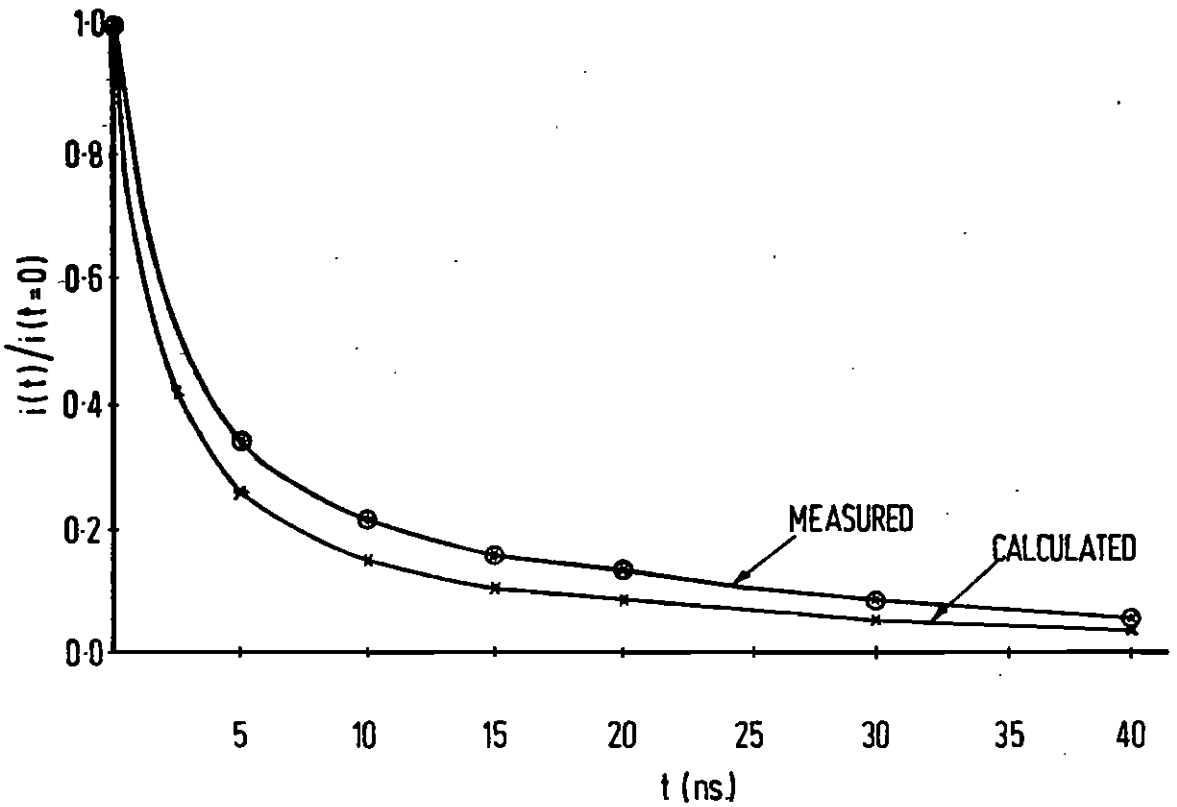
1·0
0·8
0·6
0·4
0·2
0·0
i(t)/i(t=0)
MEASURED
CALCULATED
5
10
15
20
25
30
35
40
t (ns)

Fig. 2

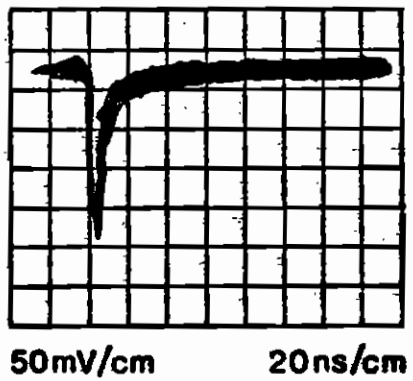

Fig. 3

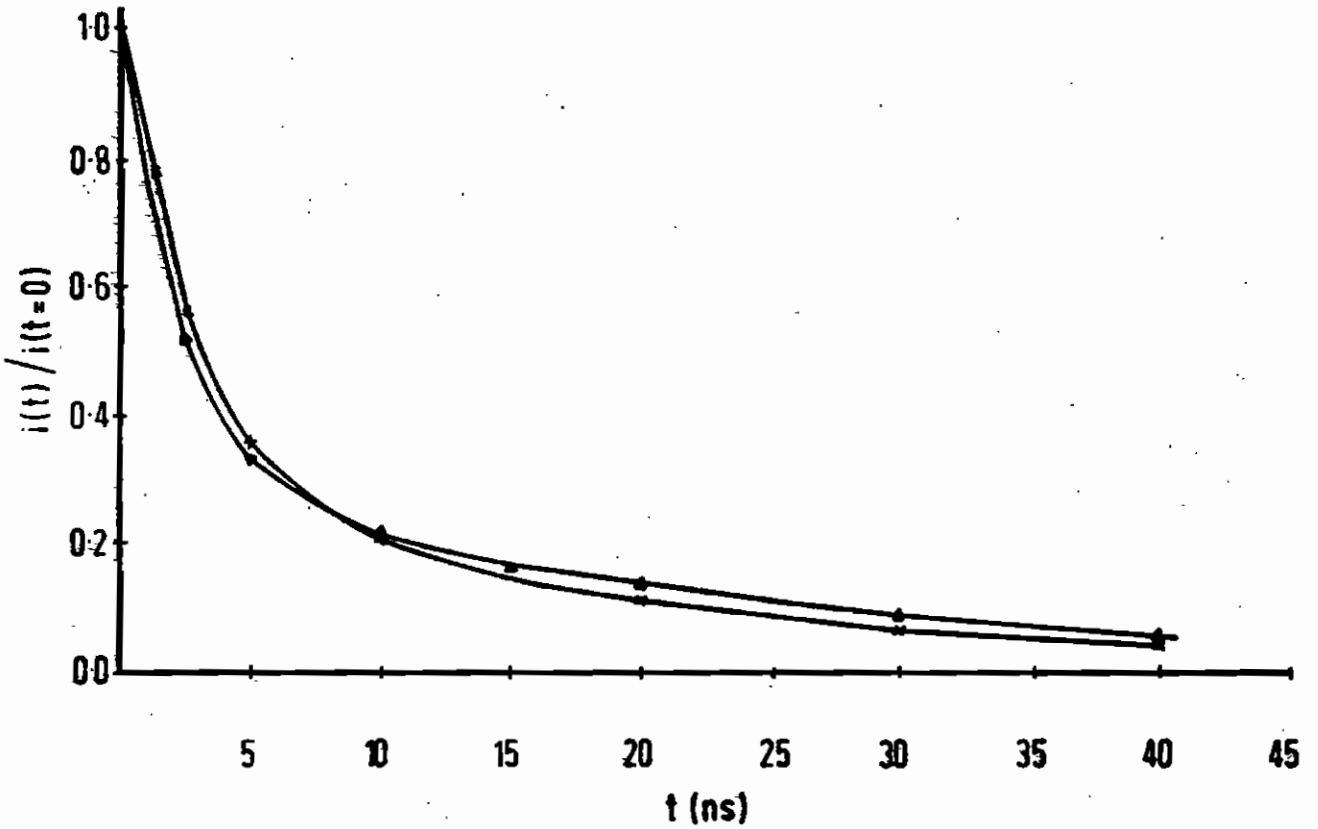

Fig. 4

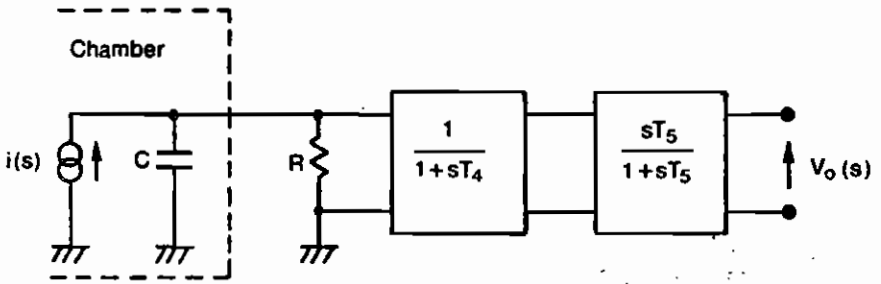
Chamber
i(s)
C
R
1
1+sT4
sT5
1+sT5
Vo (s)

Fig. 5

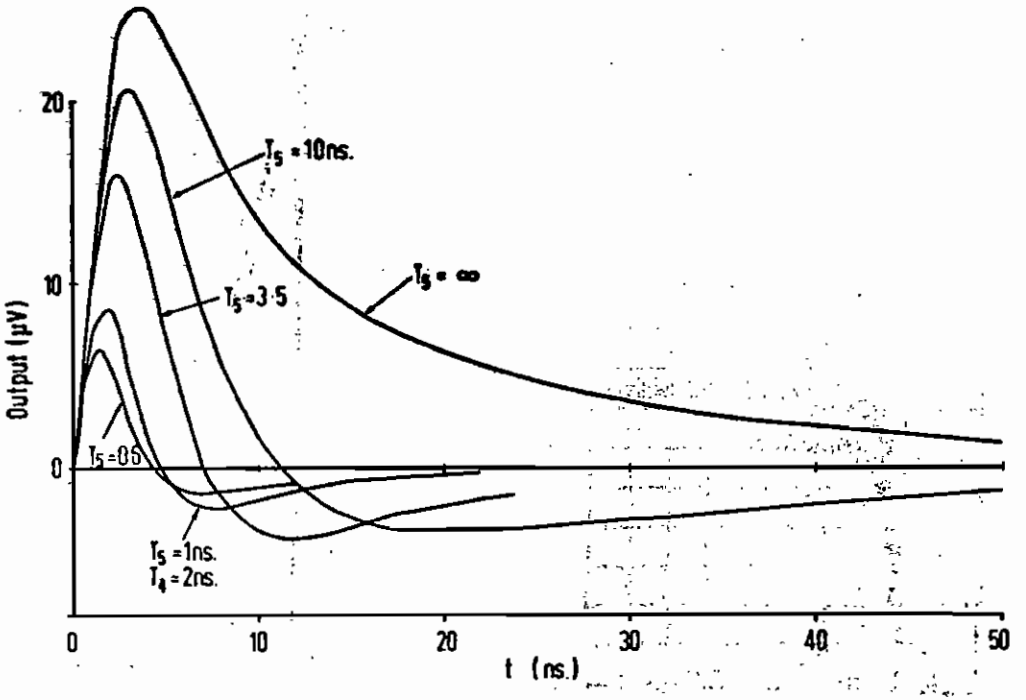
Output (μV)
20
10
0
T5 = 10ns.
T5 = 3·5
T5 = ∞
T5 = 0·5
T5 = 1ns.
T4 = 2ns.
0
10
20
30
40
50
t (ns.)

Fig. 6

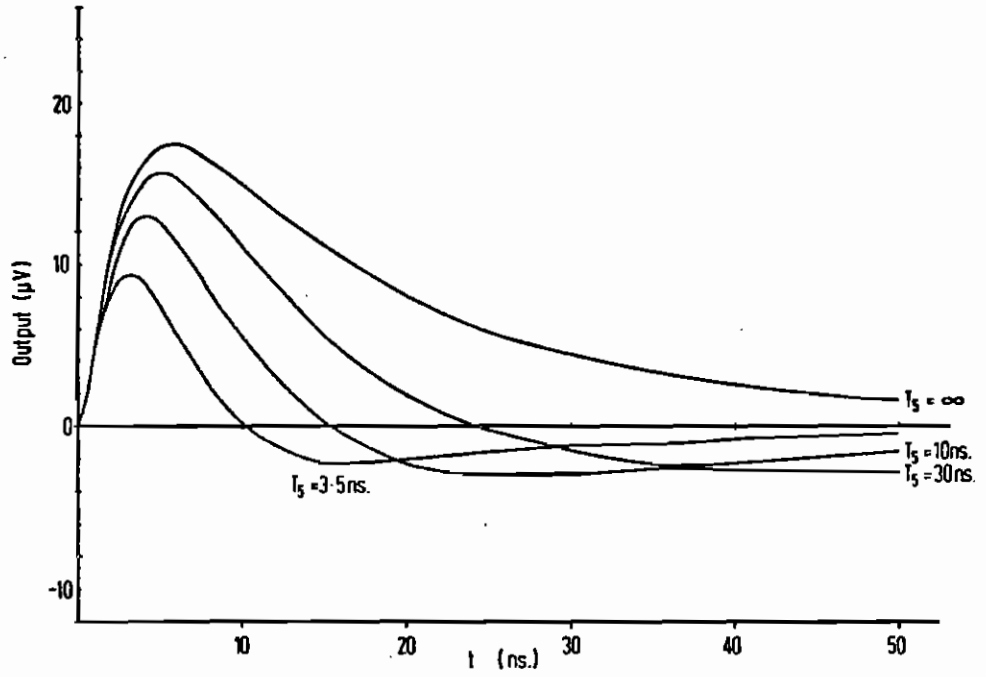
20
10
0
-10
Output (μV)
10
20
30
40
50
t (ns.)
$T_5 = \infty$
$T_5 = 10ns.$
$T_5 = 30ns.$
$T_5 = 3{\cdot}5ns.$

Fig. 7

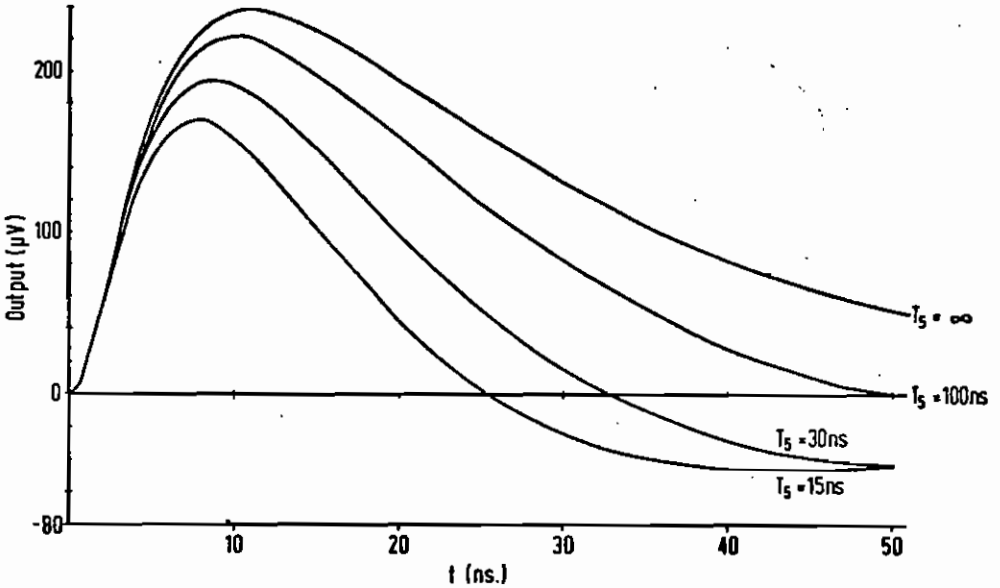
200
100
0
-80
Output (μV)
10
20
30
40
50
t (ns.)
$T_5 = \infty$
$T_5 = 100ns$
$T_5 = 30ns$
$T_5 = 15ns$

Fig. 8

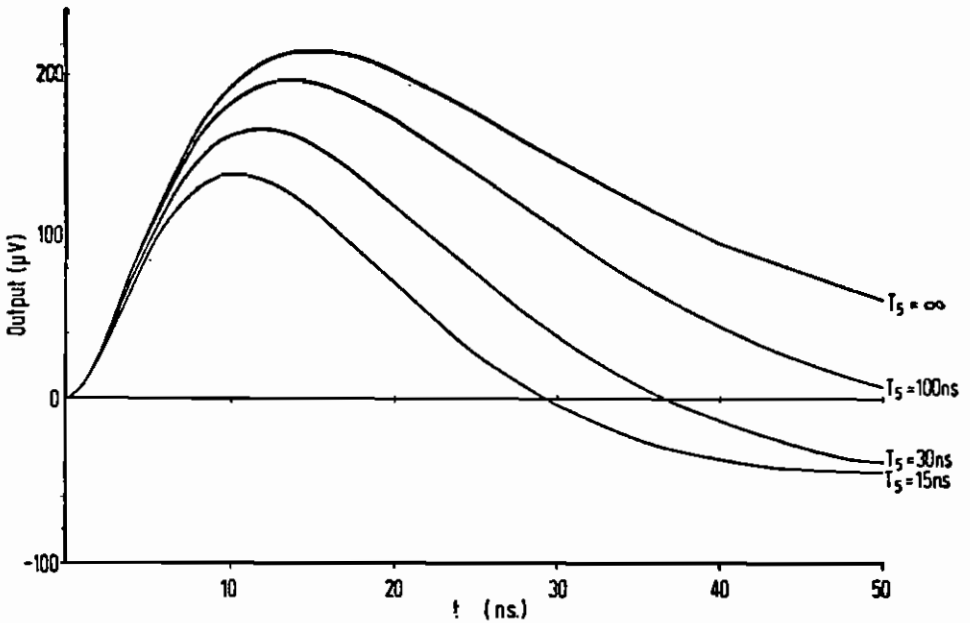
200
100
0
-100
Output (μV)
10
20
30
40
50
t (ns.)
$T_S = \infty$
$T_S = 100ns$
$T_S = 30ns$
$T_S = 15ns$

Fig. 9

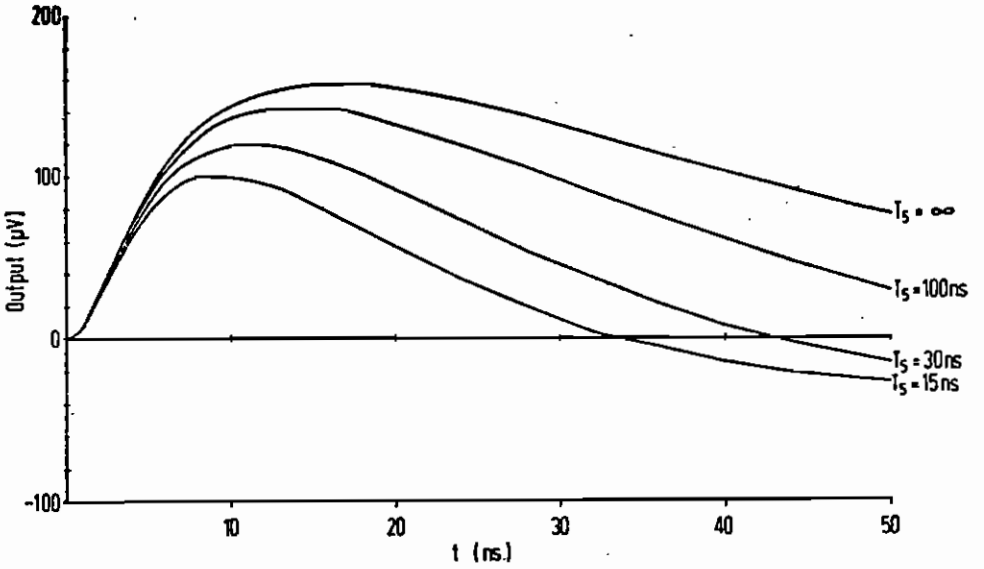
200
100
0
-100
Output (μV)
10
20
30
40
50
t (ns.)
$T_S = \infty$
$T_S = 100ns$
$T_S = 30ns$
$T_S = 15ns$

Fig. 10

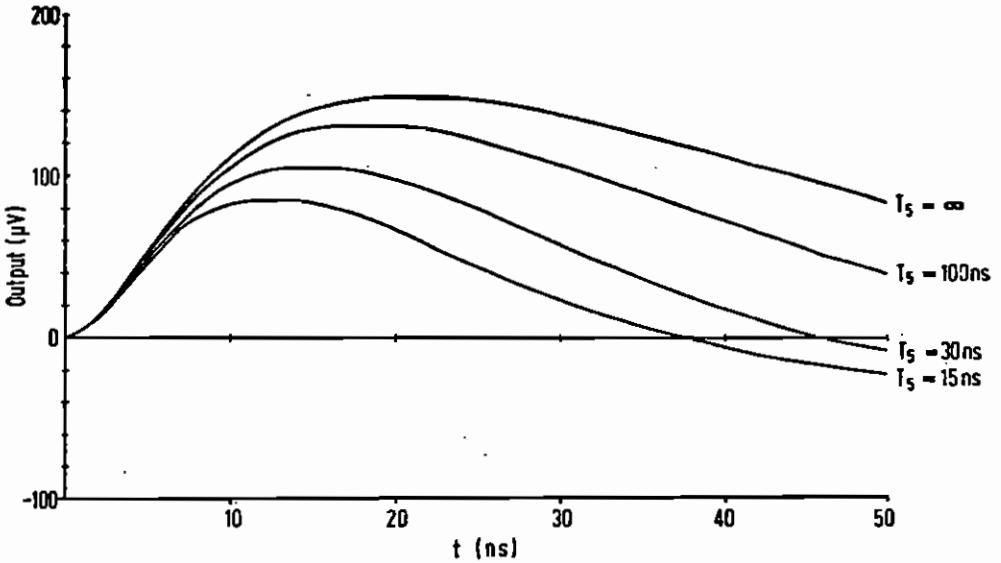
200
100
0
-100
Output (μV)
10
20
30
40
50
t (ns)
$T_S = \infty$
$T_S = 100ns$
$T_S = 30ns$
$T_S = 15ns$

Fig. 11

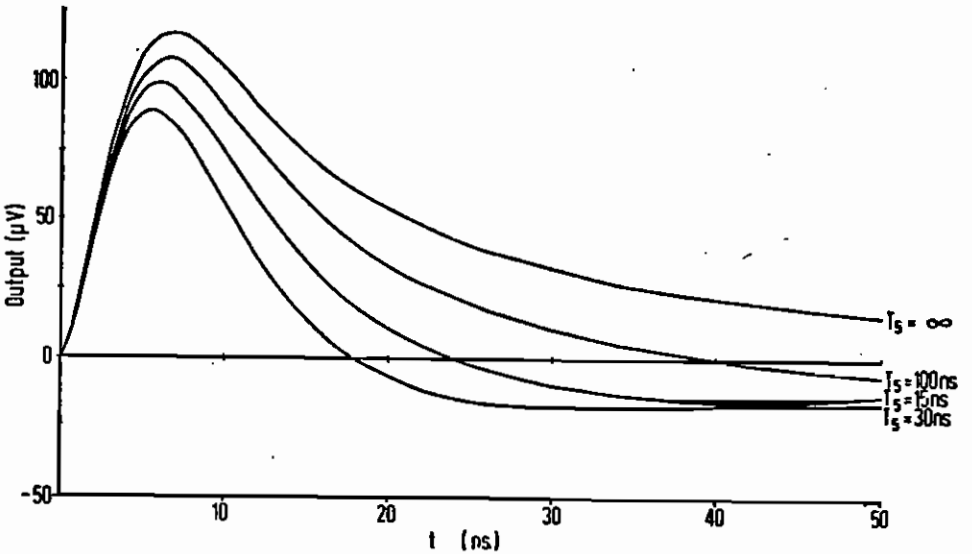
100
50
0
-50
Output (μV)
10
20
30
40
50
t (ns)
$T_S = \infty$
$T_S = 100ns$
$T_S = 15ns$
$T_S = 30ns$

Fig. 12

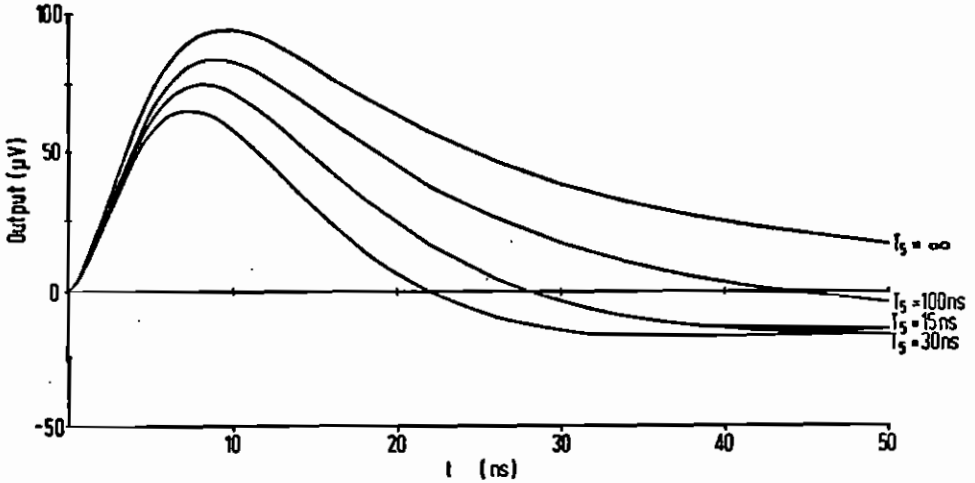
100
50
0
-50
Output (μV)
10
20
30
40
50
t (ns)
$T_S = \infty$
$T_S = 100ns$
$T_S = 15ns$
$T_S = 30ns$

Fig. 13

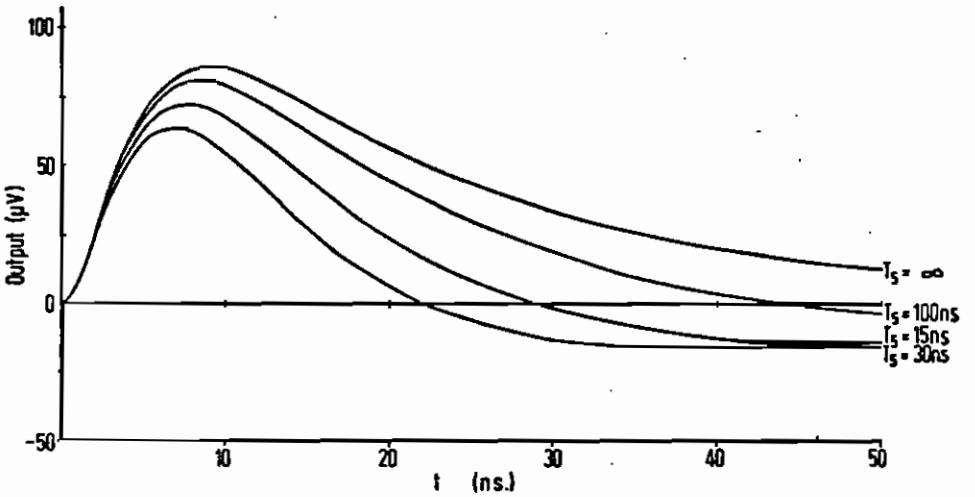
100
50
0
-50
Output (μV)
10
20
30
40
50
t (ns.)
$T_S = \infty$
$T_S = 100ns$
$T_S = 15ns$
$T_S = 30ns$

Fig. 14

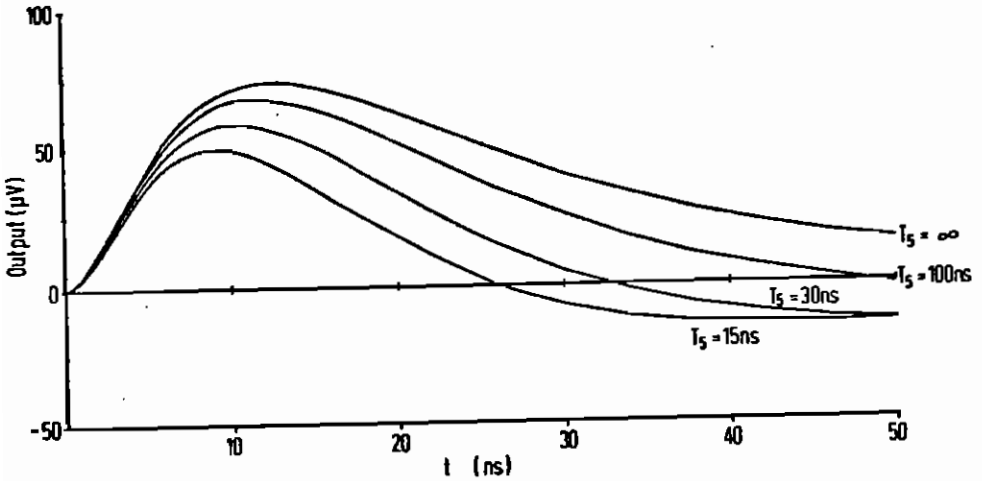
100
50
0
-50
Output (μV)
10
20
30
40
50
t (ns)
$T_5 = \infty$
$T_5 = 100ns$
$T_5 = 30ns$
$T_5 = 15ns$

Fig. 15

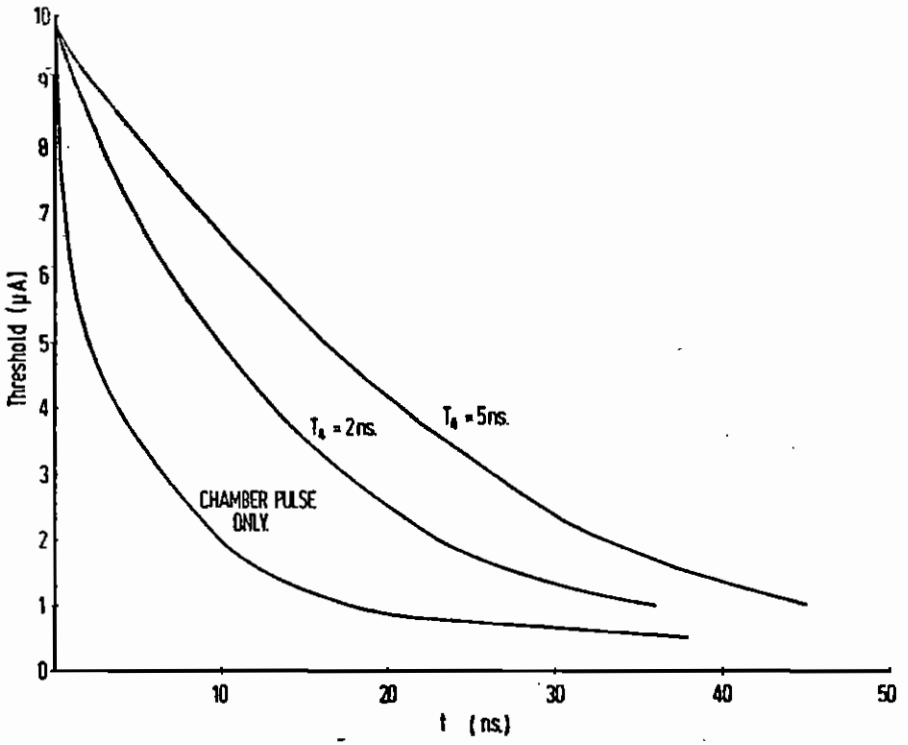
10
9
8
7
6
5
4
3
2
1
0
Threshold (μA)
10
20
30
40
50
t (ns)
$T_4 = 5ns$.
$T_4 = 2ns$.
CHAMBER PULSE
ONLY.

Fig. 16

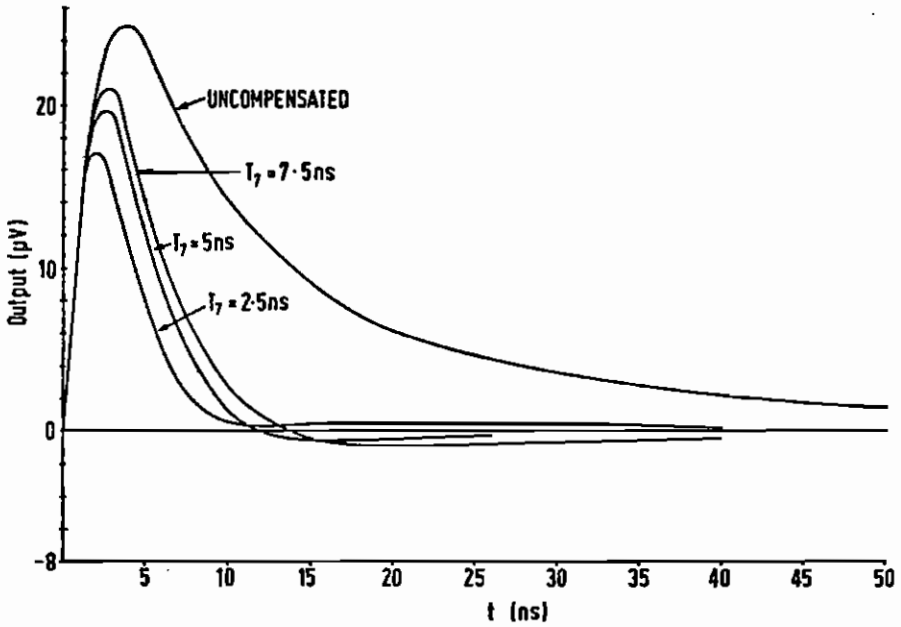

Fig. 17

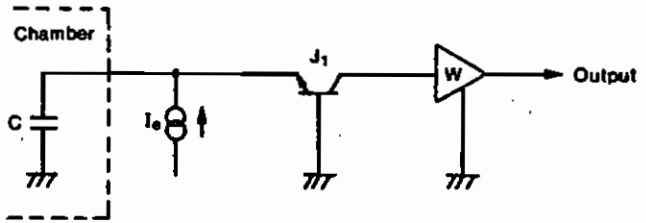

Fig. 18

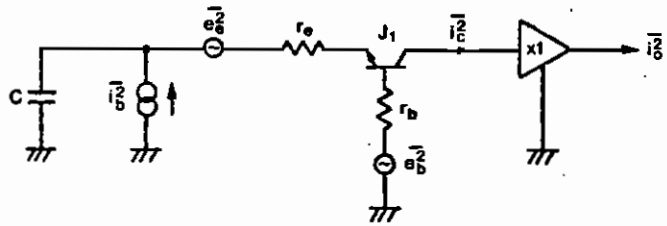

Fig. 19

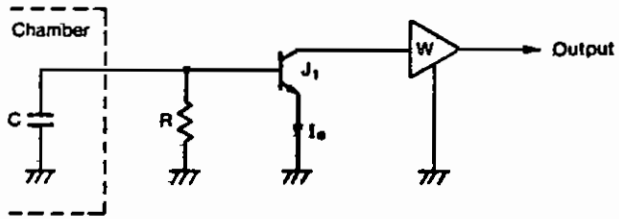

Fig. 20

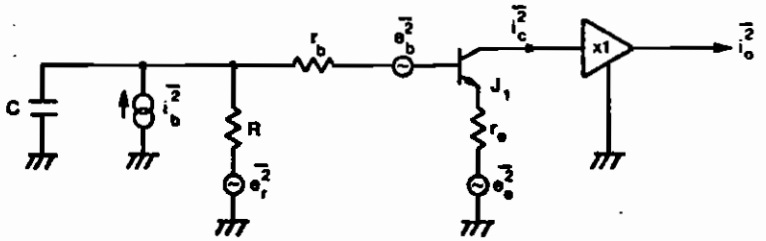

Fig. 21

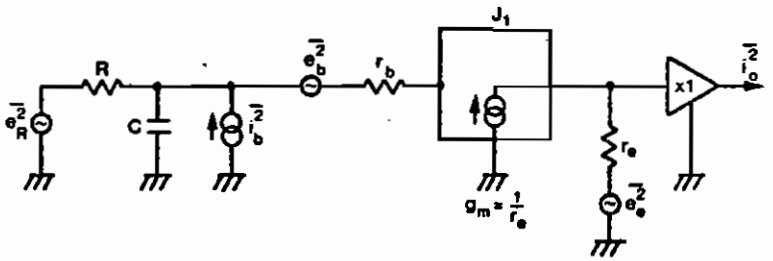

Fig. 22

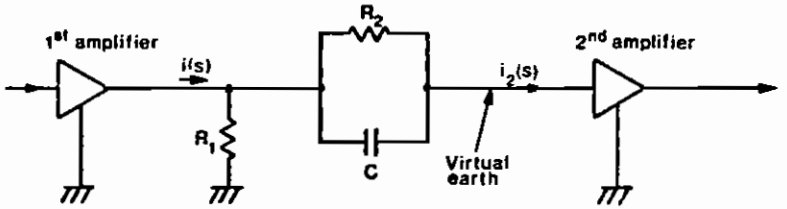

Fig. 23